Prepared for submission to JHEP

Search for magnetic monopoles with the MoEDAL trapping detector in 8 TeV proton-proton collisions at the LHC

Draft version 1.0

The MoEDAL Collaboration

(need to insert here full list of names and institutes)

Abstract: The magnetic monopole appears in theories of spontaneous gauge symmetry breaking and its existence would explain the quantisation of electric charge. The MoEDAL experiment is designed to directly search for monopoles and other highly-ionising particles produced in high-energy collisions at the LHC, based on two dedicated techniques: nuclear-track detectors sensitive to high-ionisation signatures, and a monopole trapping detector consisting of an array of aluminium samples which are then analysed for magnetic charge with a superconducting magnetometer. A trapping detector prototype was exposed to 8 TeV proton-proton collisions for an integrated luminosity of $0.75\ \mathrm{fb}^{-1}$ in 2012. Results from this run are presented, providing for the first time a direct measurement of the magnetic charge carried by particles produced in LHC collisions. No magnetic charge is detected in any of the samples and the results are interpreted for monopoles in the mass range 100 GeV$\leq m \leq$ 3500 GeV and in the charge range $1g_{\mathrm{D}} \leq |g| \leq 6g_{\mathrm{D}}$, where g_{D} is the Dirac charge. Model-independent limits are presented in fiducial regions of monopole energy and direction, and model-dependent limits are obtained in scenarios of Drell-Yan monopole pair production.

Keywords: new physics, high-energy collisions, magnetic monopole, superconducting magnetometer, persistent current

Contents

1 Introduction

The existence of free magnetic charges (magnetic monopoles) would add symmetry to Maxwell's equations of electromagnetism. In 1931, Dirac showed that electric charge quantisation could be explained as a natural consequence of angular momentum quantisation in the presence of a magnetic monopole [1]. In 1974, 't Hooft and Polyakov independently demonstrated that a grand unification theory with the U(1) subgroup of electromagnetism embedded into a larger gauge group which becomes spontaneously broken by the Higgs mechanism automatically possesses a topological magnetic monopole solution [2, 3]. It was also proposed that magnetic monopole solutions could arise within the electroweak theory itself [4], which also relies on spontaneous gauge symmetry breaking. This so-called electroweak monopole would have a mass of the order of several TeV [5], possibly within reach of the LHC.

It follows from Dirac's argument that the magnetic charge q_m carried by a monopole should be an integer multiple of the fundamental Dirac magnetic charge. In Gaussian units, the Dirac quantisation relation reads:

$$\frac{q_m}{e} = \frac{n}{2\alpha_{\mathrm{e}}} = n \cdot g_{\mathrm{D}} \approx n \cdot 68.5, \tag{1.1}$$

where e is the elementary electric charge and α_{e} is the fine structure constant. In SI units, the dimensionless quantity g is related to the magnetic charge q_m by the relation $q_m = gec$ (similarly as for the electric charge, where $q_e = ze$).

The Dirac magnetic charge g_{D} is obtained for $n = 1$ assuming the electron charge as the fundamental electric charge. Its large value, $g_{\mathrm{D}} = 68.5$, implies that the minimum coupling of a monopole to the photon should be much larger than 1, precluding perturbative calculations of monopole production processes. The minimum value of the magnetic charge quantisation number is g_D according to Dirac, $2g_D$ according to Schwinger [6] and also generally in cases where the monopole is topological such as the grand-unification monopole [2] and the electroweak monopole [4], and $3g_D$ or $6g_D$ if one considers the elementary charge to be carried by the down-quark. The lightest magnetic monopole would be stable by virtue of magnetic charge conservation. In terms of in-flight ionisation energy loss at high velocity, a monopole with the Dirac charge corresponds to an electrically charged particle with charge $|z| \approx 68.5$, corresponding to energy losses in matter over 4500 times higher than a muon [7–9]. At colliders, monopoles would be produced in pairs and manifest themselves as very highly ionising particles, quickly slowing down and stopping in exposed material around the interaction points. They would be expected to remain trapped in the material owing to a high binding energy between monopoles and nuclei with non-zero magnetic moments [10]. One way to identify a free magnetic charge trapped in matter is to measure the persistent current it would induce when passed through a superconducting loop.

Three kinds of techniques were commonly used at past colliders: (1) General-purpose detectors with high ionisation energy loss detection capabilities (e.g. OPAL at LEP [11] and CDF at the Tevatron [12]); (2) dedicated nuclear-track detectors [13] deployed around the interaction points (e.g. at LEP [14, 15] and at the Tevatron [16]); and (3) the induction technique applied to accelerator and detector material in which monopoles may have stopped and remained trapped (e.g. at HERA [17] and at the Tevatron [18, 19]). Together, these searches excluded the presence of monopoles with charge equal to or above the Dirac charge and masses up to 400 GeV. Masses higher by one order of magnitude (up to 4 TeV) can be probed at the LHC. For optimum results, the LHC programme should include all three of these complementary techniques [20]. An initial monopole search was performed at the ATLAS general-purpose experiment, excluding masses up to the order of 1 TeV assuming Drell-Yan cross sections extrapolated to high electromagnetic charges, for magnetic charges up to $|g| = 1.5g_D$ and electric charges up to $|z| = 60$ [21, 22]. Monopole trapping experiments were shown to be feasible at the LHC [23]. The dedicated MoEDAL experiment [24] uses a combination of in-flight detection with nuclear-track detectors and trapping with aluminium absorbers. MoEDAL has the great advantages of a lower average material budget along the particle path, the lack of electronics, and the possibility to calibrate directly its detectors for high particle charges with minimal assumptions and well-controlled systematics. These virtues allow to probe higher charges and masses in a robust manner. In this paper, we present results from the MoEDAL trapping detector prototype deployed in 2012 and exposed to 8 TeV collisions.

2 The MoEDAL trapping detector

The MoEDAL detector is dedicated to searches for new physics featuring long-lived particle signatures at the LHC. It is deployed around the intersection region at Point 8 of the LHC in the LHCb experiment's VELO (VErtex LOcator) [25] cavern. It is a unique and largely passive LHC detector currently comprised of four sub-detector systems [24]. Two subdetectors are arrays of nuclear-track detectors in stacks of two different compositions, optimised for different particle charge ranges. One subdetector is an array of TimePix pixel devices devoted to the monitoring of highly-ionising backgrounds in the MoEDAL cavern. Finally, the fourth subdetector is the trapping detector, providing the unique capability to capture long-lived charged particles for subsequent analysis at a remote instrumented facility.

The 2012 MoEDAL trapping detector prototype was an aluminium volume comprising 11 boxes each containing 18 cylindrical rods of 60 cm length and 2.5 cm diameter. The choice of material is driven by several factors: aluminium is cheap, non-magnetic, and has a nucleus which does not activate and which, thanks to its large nuclear magnetic moment, would be expected to strongly bind with monopoles which would range out and stop within the array [10]. The boxes were stacked in two columns behind the LHCb VELO vacuum vessel just under the beam pipe. They were numbered from 1 to 11 starting from the bottom, with the eleventh box placed on top in between the two columns. The position of the centre of the top box was (x,y,z)=(0,-440 mm,-1500 mm) with an uncertainty of 10 mm for each coordinate. The full array covered 1.3% of the total solid angle. Fig. 1 summarises the geometry of the detector and its surroundings and quantifies the amount of material in radiation lengths (X0) present in the installation. The material budget between the interaction point and the trapping detector varied from 0.1 to 8 X0 depending on position, on average 1.3 X0, with main contributions from the VELO vacuum vessel interior and outer wall, a vacuum pump, and vacuum manifold components attached to the VELO vessel. These elements were implemented in a geometry model, using the LHCb geometry model as a basis. In addition, for modelling the cables and pipes, the approximation of a grid of material was used, with 101 vertical rods of radius 3.0 mm, spaced out in a 10 mm grill at $z = -1150$ mm. This represents on average 2.3% of the total radiation length. To model material uncertainties, geometries with conservatively small and large amounts of material are defined by changing the grid rod radius to 0.1 mm and 5.0 mm, respectively. Simulations of monopole propagation in matter are described in Section 4.

The 2012 trapping detector array was exposed to an integrated luminosity of 0.75 fb^{-1} of 8 TeV proton-proton collisions. After the run was finished, the rods were retrieved and cut into samples of 20 cm length (except for the top box, whose rods were cut into a mix of 10, 15, 20 and 30 cm samples for studying the sample size dependence of the magnetometer response), for a total of 606 samples.

3 Magnetometer measurements

A DC-SQUID rock magnetometer (model 755) housed at the Laboratory for Natural Magnetism at ETH Zurich was used for scanning the trapping detector samples. Previous studies performed with rocks and with a small set of material samples from the LHC accelerator demonstrated that this instrument has the capability to detect monopoles trapped in matter with charges much less and much larger than the Dirac charge [23, 26]. The magnetometer calibration was performed with a convolution method applied to a dipole sample, and cross-checked using long thin solenoids which mimic a monopole of well-known magnetic charge [23]. The magnetometer response was found to be linear and charge sym-

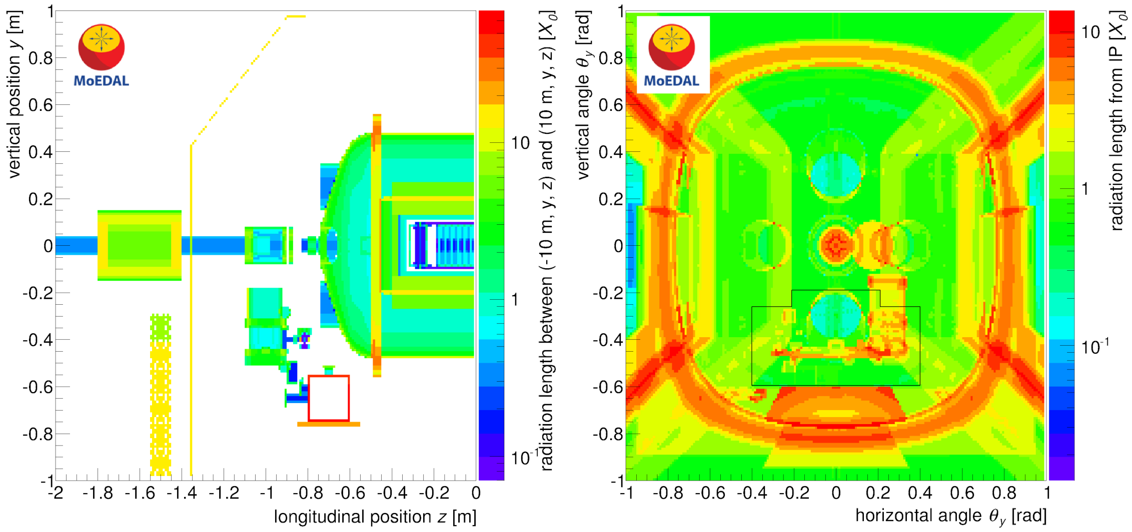

Figure 1. Material budget in radiation length in the yz plane for $|x| < 2$ m (left) *currently 10 m (?) to be changed* and in the $\theta_x\theta_y$ plane for $z = -1.45$ m (right) *y on horizontal axis should be changed to x*. In the right figure, the outline of the trapping detector (placed just beyond the considered range for material integration) is indicated in black. The grid used as an approximation to model cables and pipes is not included in these figures.

metric. After calibration, the measured current is translated into units of current expected from the passage of a Dirac magnetic charge, I_{g_D}.

Each of the 606 aluminium samples of the trapping detector was passed at least once through the magnetometer, mostly during a measurement campaign in September 2013. Every tenth measurement on average was performed with an empty sample holder for offset subtraction. Measurements with one 20 cm sample at 76 different positions before, during and after passage through the sensing coils, after subtracting the same measurements with an empty sample holder, are shown in Fig. 2. This provides an example of a typical magnetometer response profile as a function of sample position. An emulation of the response expected if a north or south monopole was present in the sample is given in the figure by adding or subtracting measurements obtained with a long solenoid scaled to the current expected from a Dirac monopole I_{g_D}. With a monopole present, the last measured value would differ significantly from the first value. The monopole signature is therefore measured in terms of a quantity called persistent current, defined as the difference between the currents measured after and before passage of the sample through the sensing coil, from which the same difference obtained with a nearby empty holder measurement is subtracted. Whenever the persistent current differed from zero by more than $0.25g_\mathrm{D}$ — spurious jumps caused this to happen in $\sim$2% of the measurements — the sample was considered a candidate and measured again several times. Such jumps, called flux jumps, are known to happen when the SQUID flux-locked loop is temporarily lost and regained at another quantum level [27]. A sample containing a genuine monopole would consistently

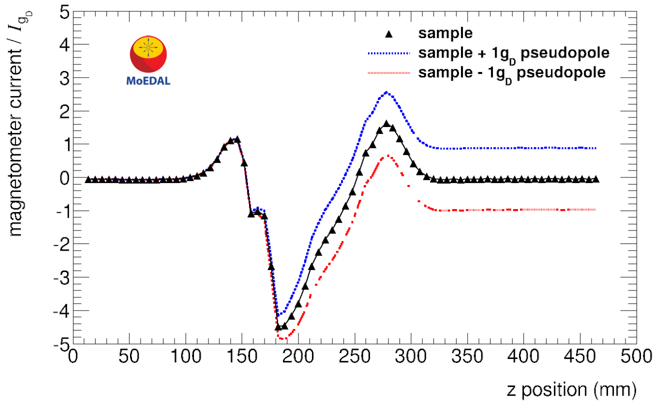

Figure 2. Magnetometer response profile for a typical aluminium sample of the trapping detector, after subtracting the response obtained with an empty sample holder. The dashed lines show the responses when the measurement from a long solenoid (pseudopole) is added and subtracted to emulate the presence of a Dirac monopole in the sample.

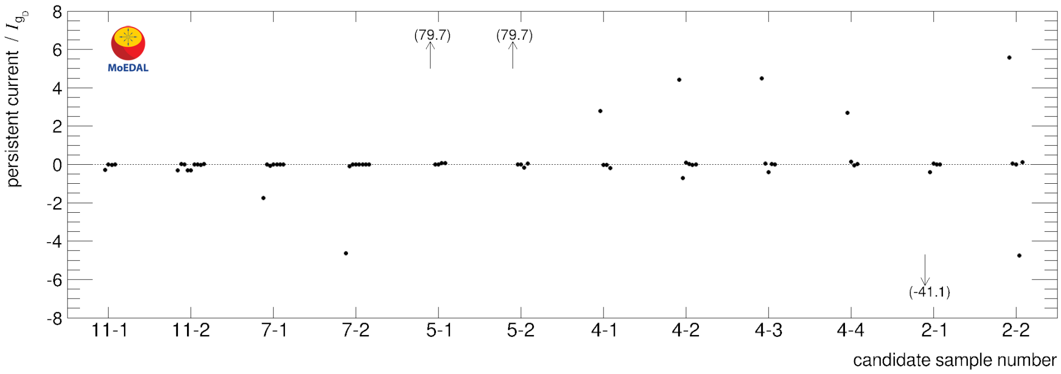

Figure 3. Results of multiple persistent current measurements (in units of the Dirac charge) for the 12 samples which yielded large ($|g| > 0.25\ g_D$) values for the first measurement.

yield the same value for repeated measurements, while values repeatedly consistent with zero are expected whenever an instrumental effect occurred in the first measurement. Including first and multiple sample measurements as well as empty holder and calibration measurements, a total of 852 independent measurements were performed in 7 days.

Multiple measurements of potential candidates are shown in Fig. 3. In all cases where the first measurement showed a large fluctuation, additional measurements of the same sample were consistent with zero. It was noticed that jumps occurred more often for certain periods during which the magnetometer response was less stable than usual. Such instabilities can be caused by several known instrumental and environmental factors: flux jumps occurring when the slew rate is increased [27] as, for instance, when a large sample is passed through the sensing coil at a high speed, noise currents in the SQUID feedback

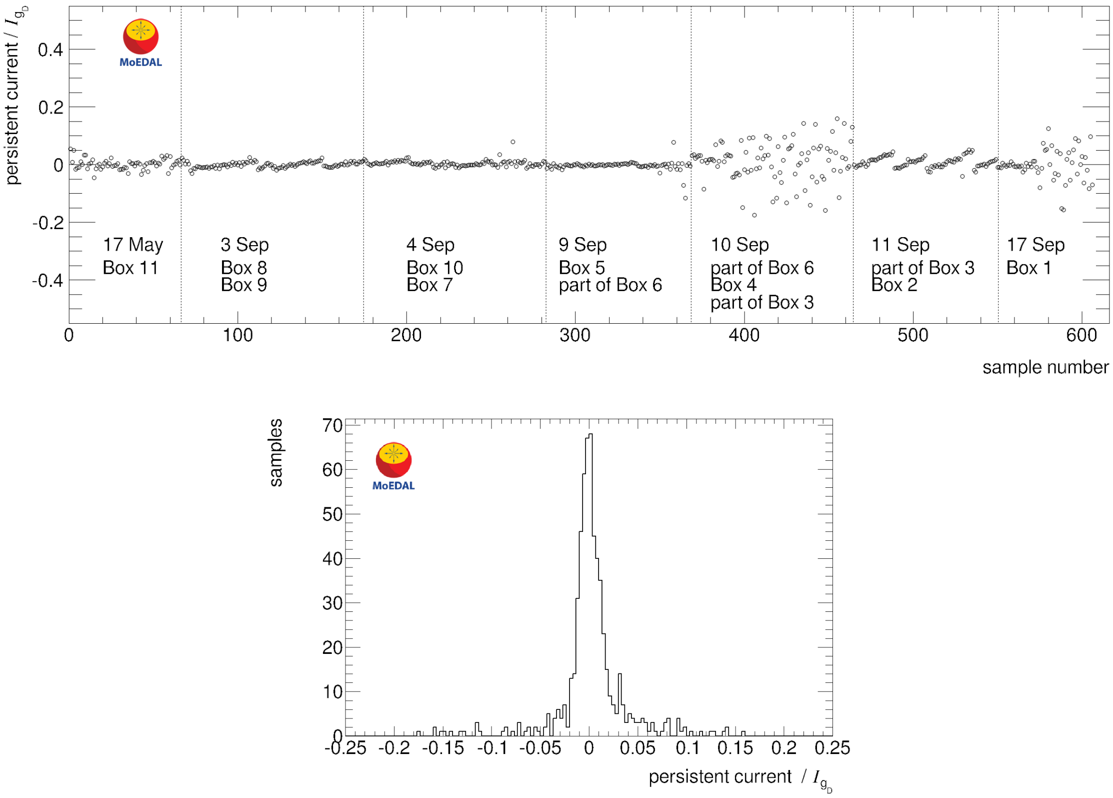

Figure 4. Magnetic charge (in units of the Dirac charge) measured in the 606 aluminium samples of the 2012 MoEDAL trapping detector.

loop, small (∼mm) variations in the length of the sample holder from one run to another, the accumulation of condensed water and ice in the magnetometer tube near the cold sensing region, physical vibrations and shocks, and variations in external magnetic fields, in particular the geomagnetic field but also possibly fields from high-voltage power line activity in the vicinity of the laboratory. With experience, measures can be taken to try to minimise such effects when performing measurements.

The magnetic charge contained in all 606 samples of the trapping detector — as measured by the first measurement or a subsequent measurement in the cases where a spurious offset jump was observed for the first measurement — is shown in Fig. 4. The top plot gives an idea of the evolution of the resolution with time, where periods of relative instability are observed for the 10th and 17th of September. The saw tooth feature most clearly visible for 11th of September is due to a lack of available empty holder measurements, causing less frequent offset drift corrections. The bottom plot shows the data as a histogram. No measurements yield values of $|g|$ beyond $0.18g_{\rm D}$. The probability that a sample containing a genuine monopole with $|g| \geq 0.5g_{\rm D}$ would yield a persistent current lower than $0.25g_{\rm D}$ so as to remain unnoticed is estimated to be less than 0.5%. Thus, the presence of monopoles with $|g| \geq 0.5g_D$ is excluded.

4 Monopole simulations

Heavy monopole pair production from the initial pp state is modelled by quark-antiquark annihilation into a virtual photon using the MadGraph5 Monte-Carlo event generator [28]. This leading-order Drell-Yan (DY) process is generated either for spin-1/2 or spin-0 monopoles. The monopole coupling to the Z boson is set to zero. For the parton distribution function of the proton, `NNPDF23_lo_as_0130` is used [29]. Examples of the resulting distributions in the plane described by the longitudinal kinetic energy $E_z^{kin} = E^{kin} \cdot \sin(\theta)$ and polar angle θ – the two chosen kinematic variables for defining trapping detector fiducial acceptances – are shown in Fig. 5. Pythia [30] is used for the initial-state radiation and the hadronisation and the underlying event. Single-monopole samples are also generated to obtain model-independent results. They are produced with a flat kinetic energy distribution ranging from 0 to 10000 GeV, and flat θ and ϕ distribution which encompass the angular acceptance of the trapping detector, i.e., 2.4 rad $< \theta <$ 3.0 rad and -2.7 rad $< \phi < -0.5$ rad. The DY and single-monopole samples are produced for masses m equal to 100, 500, 1000, 2000, 3000, and 3500 GeV and charges $|g|$ equal to 1, 2, 3, 4, 5 and 6 g_{D}, with $2 \cdot 10^6$ monopoles in each sample. For the assessment of systematic uncertainties, single-particle samples are simulated three times using three different geometries, corresponding to the baseline, minimum and maximum material.

Monopole energy loss and stopping in the material inside and around the LHCb VELO vacuum vessel and inside the trapping detector itself (see Section 2) is simulated using the GEANT4 toolkit [31]. The velocity dependence of the energy loss per unit distance is modelled by the Bethe-Bloch formula modified for monopoles [7]:

$$-\frac{\mathrm{d}E}{\mathrm{d}x} = K\frac{Z}{A}g^2\left[\ln\frac{2m_ec^2\beta^2\gamma^2}{I} + \frac{K(|g|)}{2} - \frac{1}{2} - B(|g|)\right] \tag{4.1}$$

where Z, A and I are the atomic number, atomic mass and mean excitation energy of the medium, $K = 0.307$ MeV g^{-1}cm^2, m_e is the electron mass and $\gamma = 1/\sqrt{1-\beta^2}$. The Kazama, Yang and Goldhaber cross section correction and the Bloch correction are given by $K(|g|) = 0.406$ (0.346) for $|g| = g_D$ ($2g_D$) and $B(|g|) = 0.248$ (0.672, 1.022, 1.685) for $|g| = g_D$ ($2g_D$, $3g_D$, $6g_D$) [7]. Equation 4.1 is not valid for velocities $\beta \leq 0.01$, where the approximation $-\mathrm{d}E/\mathrm{d}x = (45\ \mathrm{GeV/cm})(g/g_D)^2\beta$ [9] is used for all materials. Effects from theoretical uncertainties in the $\mathrm{d}E/\mathrm{d}x$ calculations are neglected since they are estimated to be much smaller than effects from uncertainties in the material budget. Due to the large monopole masses considered, energy losses from bremsstrahlung and pair production, which are important only for highly relativistic particles, are negligible compared to ionisation. Monopole accelaration along magnetic field lines is implemented in the model but irrelevant in this case, as the MoEDAL trapping detector is located in a region of the cavern where the magnetic field is negligible.

The acceptance of the trapping detector, defined on an event basis as the probability that at least one monopole stops inside one of the aluminium rods, is determined by propagating monopoles into the geometry model. The acceptance is clearly highly dependant on the energy distribution predicted by the model and on the material budget in front of

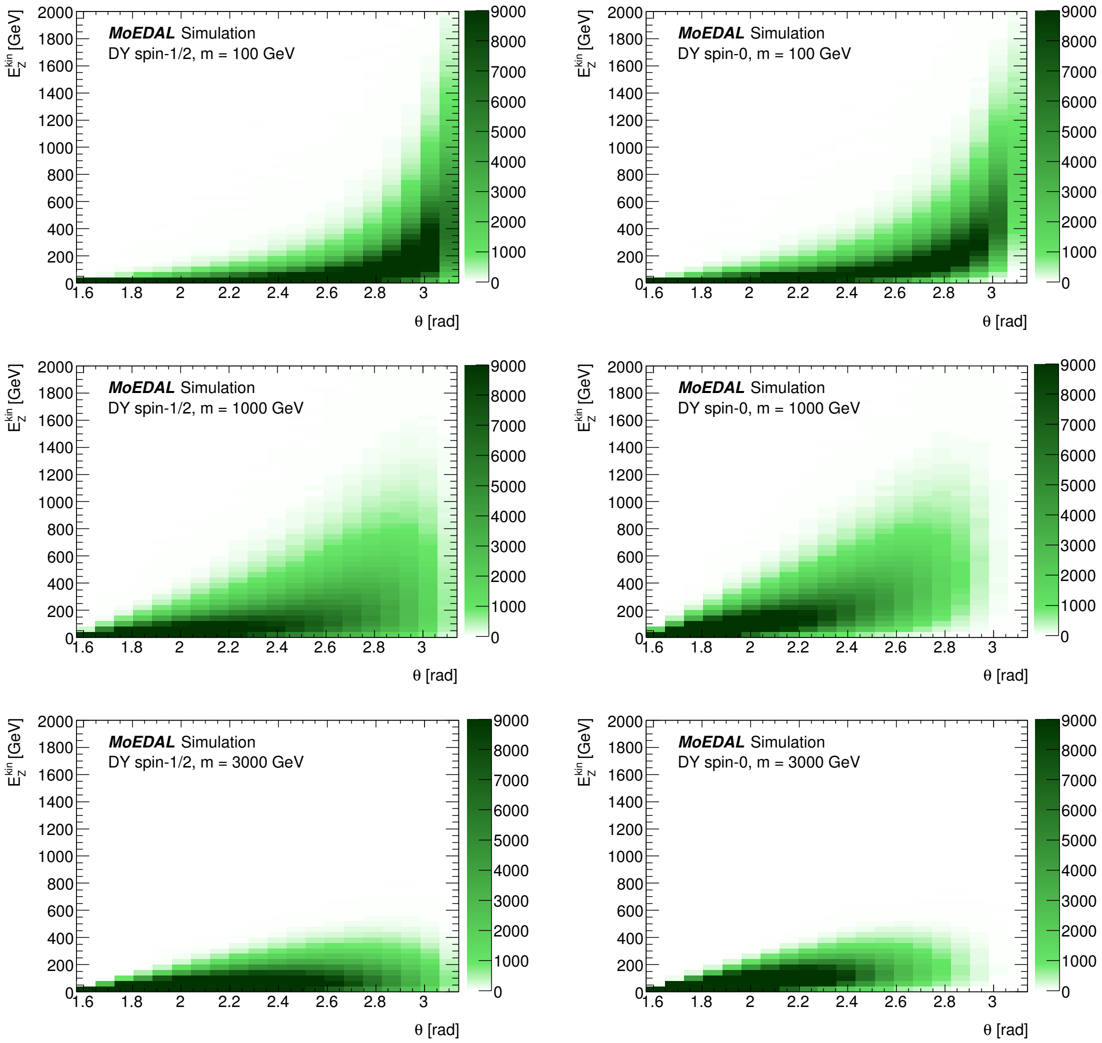

Figure 5. Generator-level distributions of monopoles produced in the Drell-Yan model in the plane described by the longitudinal kinetic energy E_z^{kin} and polar angle θ, for spin-1/2 (left) and spin-0 (right) monopoles with mass 100 GeV (top), 1000 GeV (middle) and 3000 GeV (bottom), using 10^6 events for each sample. These distributions do not depend on monopole charge. The distribution in the range $0 < \theta < \pi/2$ is symmetric to the one which is shown here.

the detector. Monopoles with low charges and high energies tend to punch through the trapping material and are thus better captured in regions where they are slowed down by thicker upstream material. Monopoles with higher charges and low energies tend to stop before they reach the trapping detector, and are thus only trapped in regions of low upstream material. Also, for the same charge at the same kinetic energy, monopoles with lower masses possess a higher velocity, leading to higher $\mathrm{d}E/\mathrm{d}x$, and thus tend to stop earlier. For instance, a $|g| = 2g_{\mathrm{D}}$ monopole with $m = 100$ GeV needs about 100 GeV more kinetic energy to reach the trapping detector than for $m = 1000$ GeV.

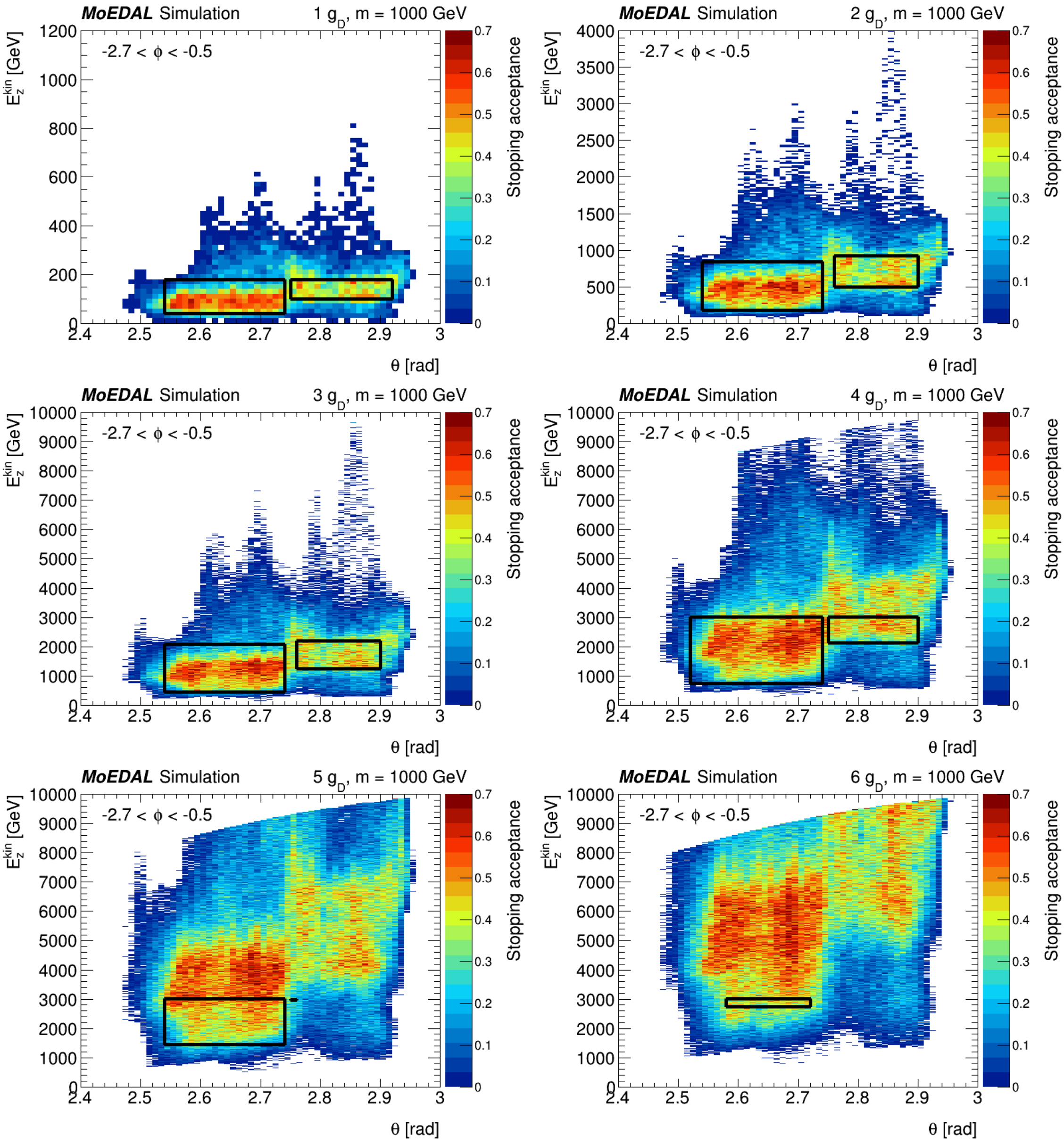

Figure 6. Trapping acceptance as a function of longitudinal kinetic energy E_z^{kin} and polar angle θ (with -2.7 rad $< \phi < -0.5$ rad), for monopoles with mass 1000 GeV and charges ranging from $1g_{\rm D}$ (top, left) to $6g_{\rm D}$ (bottom, right). The fiducial regions (as defined in the text) are indicated by black boxes. To remain physical, these boxes do not extend beyond the beam energy of 4000 GeV minus the monopole mass.

For a monopole possessing a given charge and mass with a given energy and direction at the origin, the acceptance is defined in an unique way which depends only on the geometry and not on the prodution model. Since the collisions are symmetric with respect to the azimuthal angle ϕ, only two kinematic variables are needed to define the acceptance in a model-independent manner [21, 32]. These two variables are chosen here as the lon-

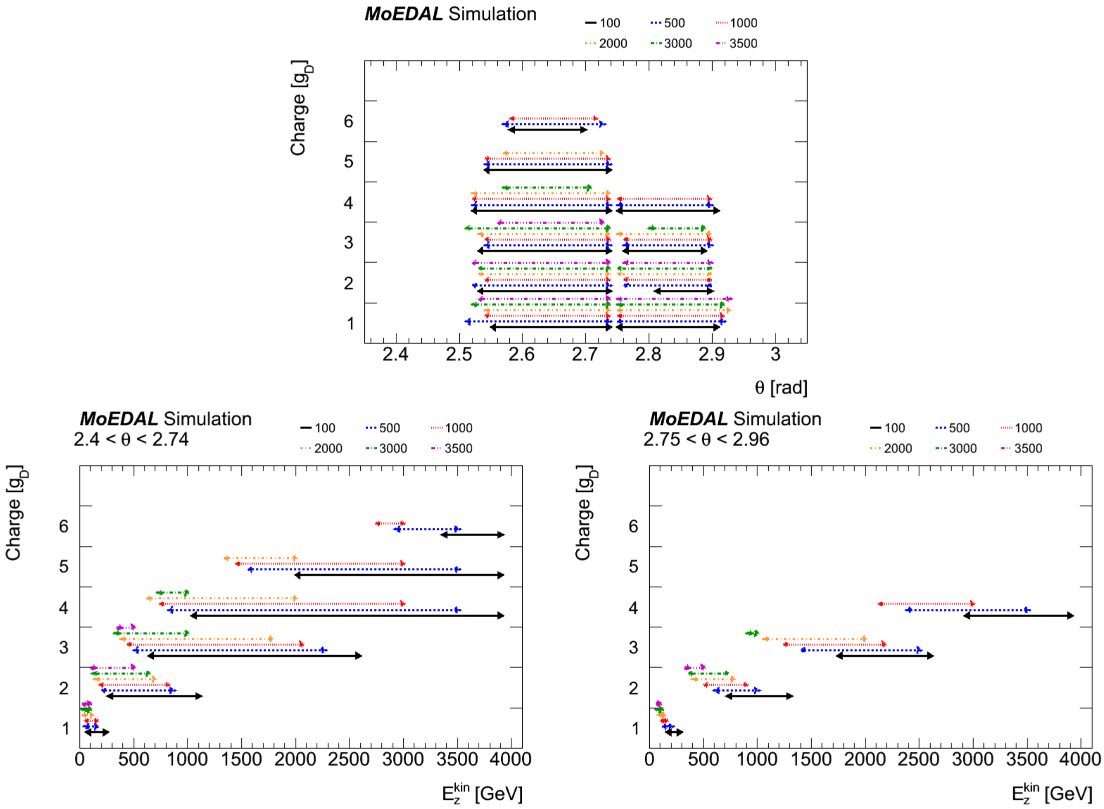

Figure 7. Graphical representation of the fiducial regions for various monopole charges and masses, defined as rectangles in the θ versus E_z^{kin} plane (with -2.7 rad $< \phi < -0.5$ rad) for which the average selection efficiency is larger than 40% with a standard deviation lower than 15%. The double arrows define the rectangle positions and dimensions, with various line styles corresponding to different monopole masses. The top plot shows the θ acceptance ranges, while the other plots show the E_z^{kin} acceptance ranges corresponding to the two different θ ranges.

gitudinal kinetic energy E_z^{kin} and the polar angle θ, after restricting the denominator of the acceptance definition to the range -2.7 rad $< \phi < -0.5$ rad (encompassing the extent of the trapping detector). Thus, using single-monopole Monte-Carlo samples, the acceptance is mapped for all mass and charge combinations as a function of E_z^{kin} and θ (with -2.7 rad $< \phi < -0.5$ rad), as shown in Fig. 6 for monopoles with $m = 1000$ GeV. These two-dimentionnal histograms contain all the information needed to obtain the acceptance in any given pair-production model to a good approximation (see below for DY). In order to present it in simple terms (at the cost of some precision, and conservatively neglecting low-acceptance regions), this information can be compactified by considering only the regions in which the acceptance is highest, which we call fiducial regions. Fiducial regions in the monopole E_z^{kin} versus θ plane are indicated by black boxes in Fig. 6. To define these regions, for each charge and mass, an automatic algorithm identifies the largest rectangle for which the average selection efficiency between all bins inside the region is larger than 0.4 with a maximum standard deviation of 15%. Another constraint is that the maximum

E_z^{kin}, to remain physically plausible for pair-produced monopoles, should not exceed the beam energy of 4000 GeV minus the monopole mass. These criteria are used in the distinct low-θ ($2.40 < \theta < 2.74$) and high-θ ($2.75 < \theta < 2.96$) regions. The ranges of θ and E_z^{kin} defining the fiducial regions found with this algorithm for all charge and mass points considered in this search (with blanck spaces in the cases where no region is found) are summarised graphically in Fig. 7, where the top plot shows the intervals in θ, the bottom left plot shows the intervals in E_z^{kin} for the low-θ region, and the bottom right plot shows the intervals in E_z^{kin} for the high-θ region.

DY acceptances are obtained in two ways. The most computationally effective way is to map the acceptance as a function of θ and E_z^{kin} (as described above and shown in Fig. 6) for each monopole mass and charge, using single-particle samples. These maps are then folded with DY pair production kinematics for both spin-1/2 and spin-0 monopoles such as the distributions shown in Fig. 5. Another way is to fully simulate pair-produced monopoles: due to computing resource limitations, such samples were produced with $2 \cdot 10^5$ events for all charge and mass points and with 10^6 events only for a selected choice of masses and charges. Comparing the results from the two methods it is observed that the folding method systematically overestimates the acceptance by $1 - 12\%$, with the largest differences seen in the cases where the acceptance region is small, as in the case of low charge ($|g| = g_{\mathrm{D}}$). This is expected due to the non-zero bin size and limited event count in each bin. The folding method is used to produce samples from which systematics from uncertainties in the material description are estimated (see below). For the acceptance estimates themselves, the fully simulated pair-produced samples are used.

The dominant source of systematics is the uncertainty in the assumed amount of material in the geometry description used by the GEANT4 simulation. *+++need assessment of effect of uncertainty in position of the array.* While the VELO vacuum vessel is modelled with great precision in the LHCb geometry, cables and pipes present on the backside of the VELO, as well as the insides of elements for which detailed technical drawings were not available (a vacuum pump and a vacuum manifold), are only approximately modelled. Therefore, two additional geometry models are used, which describe the minimum and maximum possible amounts of material assuming conservative uncertainties on material thicknesses and densities (see Section 2 for details). This results in a +++% uncertainty in the lower and higher E_z^{kin} boundaries of the fiducial regions (Fig. 7). This also results in uncertainties in DY acceptances. With $|g| = g_{\mathrm{D}}$, the resulting uncertainty is low, of the order of 1%. In the case $|g| = 2g_{\mathrm{D}}$ it is of the order of $10 - 20\%$ for intermediate masses. For higher charges, the uncertainty can become very large. It is largest for the charge and mass combinations with the lowest acceptances.

Trapping detector acceptances under the assumption of DY kinematics, including uncertainties from Monte-Carlo statistics as well as systematic uncertainties, are summarised in Table 1. This table does not include entries with acceptance lower than 0.1%, for which uncertainties can get larger than 100%. This is the case for charges $|g| \geq 5g_{\mathrm{D}}$ as well as some of the masses for charges $|g| = 3g_{\mathrm{D}}$ and $|g| = 4g_{\mathrm{D}}$, for which no interpretation is therefore attempted in the context of the DY models.

m [GeV]	$\|g\| = 1.0g_{\mathrm{D}}$	$\|g\| = 2.0g_{\mathrm{D}}$	$\|g\| = 3.0g_{\mathrm{D}}$	$\|g\| = 4.0g_{\mathrm{D}}$
spin-1/2				
100	0.026 ± 0.003	0.003 ± 0.002	—	—
500	0.019 ± 0.001	0.023 ± 0.007	0.006 ± 0.004	—
1000	0.016 ± 0.001	0.024 ± 0.005	0.008 ± 0.004	0.001 ± 0.001
2000	0.012 ± 0.001	0.022 ± 0.005	0.007 ± 0.004	—
3000	0.0158 ± 0.0005	0.011 ± 0.004	0.002 ± 0.001	—
3500	0.018 ± 0.001	0.003 ± 0.002	—	—
spin-0				
100	0.035 ± 0.001	0.007 ± 0.004	—	—
500	0.009 ± 0.001	0.028 ± 0.006	0.009 ± 0.005	0.002 ± 0.001
1000	0.0036 ± 0.0007	0.020 ± 0.002	0.010 ± 0.005	0.002 ± 0.002
2000	0.0022 ± 0.0004	0.013 ± 0.001	0.006 ± 0.003	0.001 ± 0.001
3000	0.0029 ± 0.0003	0.007 ± 0.002	0.001 ± 0.001	—
3500	0.0062 ± 0.0004	0.003 ± 0.001	—	—

Table 1. Trapping acceptances for spin-1/2 (top) and spin-0 (bottom) monopoles with DY production kinematic distributions. The quoted uncertainties include both statistical and systematic uncertainties. Empty entries mean that the acceptance is less than 0.001.

5 Limits on monopole production

A magnetic charge consistent with zero is observed in the trapping detector samples, leading to a 95% confidence level upper limit of 3 on the number of events capable of producing at least one monopole stopping and binding in the trapping detector in 0.75 fb^{-1} of 8 TeV proton-proton collisions. From this limit, using acceptance estimates and their uncertainties for the different production models (Table 1), 95% confidence level cross section limits for various monopole charge and mass hypotheses are obtained using a Bayesian method with Poisson statistics described in detail in Ref. [33]. The nuisance parameters are modeled as log-normal, and a flat prior is assumed for the cross section. These limits are valid under the assumption that a monopole which stops in the aluminium material will always be captured and remain bound to a nucleus. For monopoles produced at values of energy and direction corresponding to the fiducial regions, a 40% acceptance is used (this comes from the fiducial region definition, see Section 4 and Fig. 6), resulting in a limit of 10 fb. For DY pair production, cross-section limits are shown graphically as functions of mass in Fig. 8 and as a function of charge in Fig. 9 for spin-1/2 (top) and spin-0 (bottom) monopoles.

Theoretical production cross-sections (solid lines in Figs. 8 and 9) correspond to DY pair production cross sections of massive particles with a single electric charge at leading order, scaled by a factor $g^2 = (n \cdot 68.5)^2$. They should be considered with caution since the monopole coupling to the photon is actually too large for perturbative calculations to converge. Under the rough assumption of such monopole production cross sections, the cross section limits obtained above are used to obtain mass limits. These are shown in

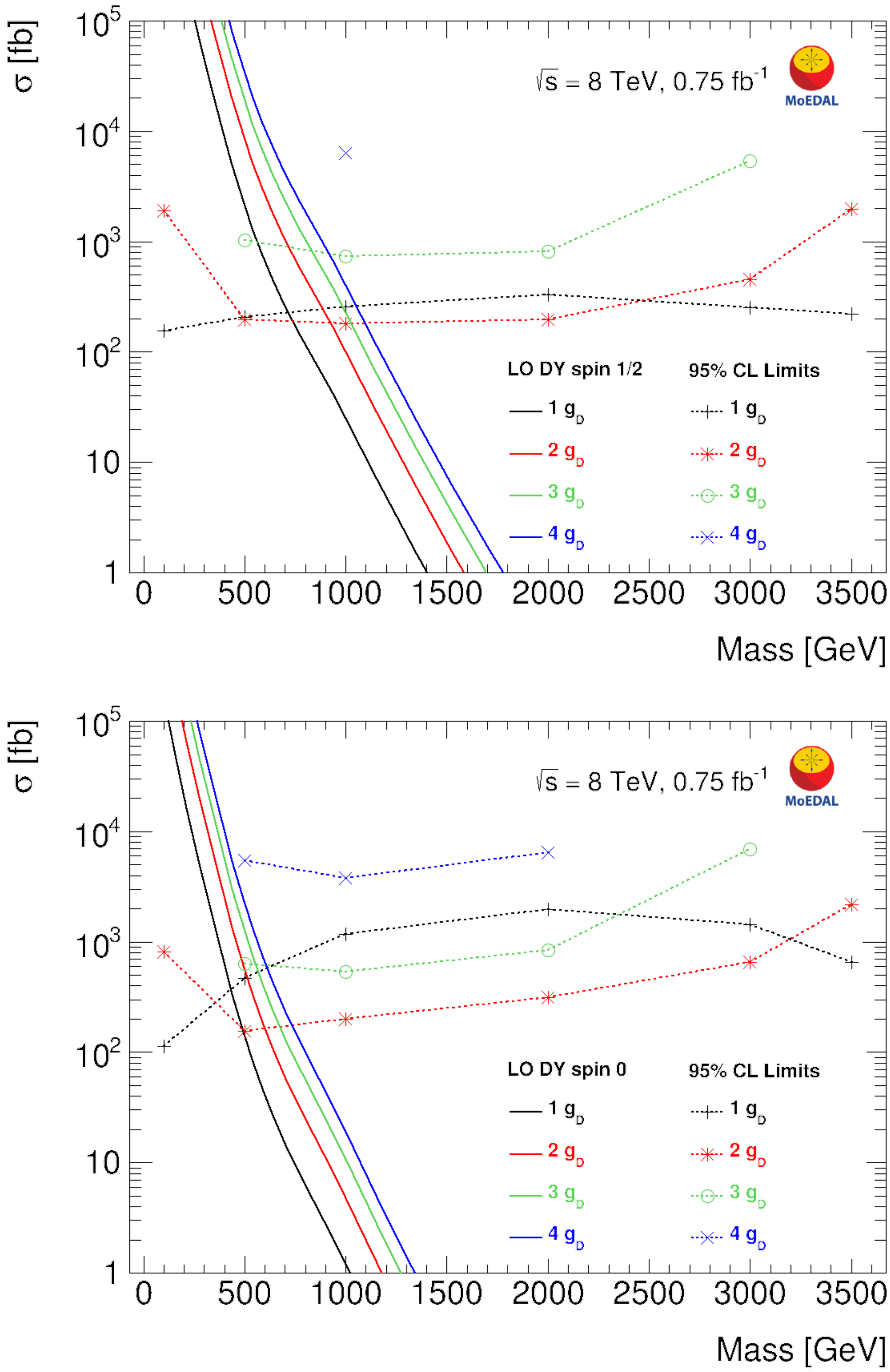

Figure 8. Cross-section upper limits at 95% confidence level for leading-order DY monopole production as a function of mass for spin-1/2 (top) and spin-0 (bottom) monopoles. The various line styles correspond to different monopole charges. The solid lines are DY cross section calculations at leading order.

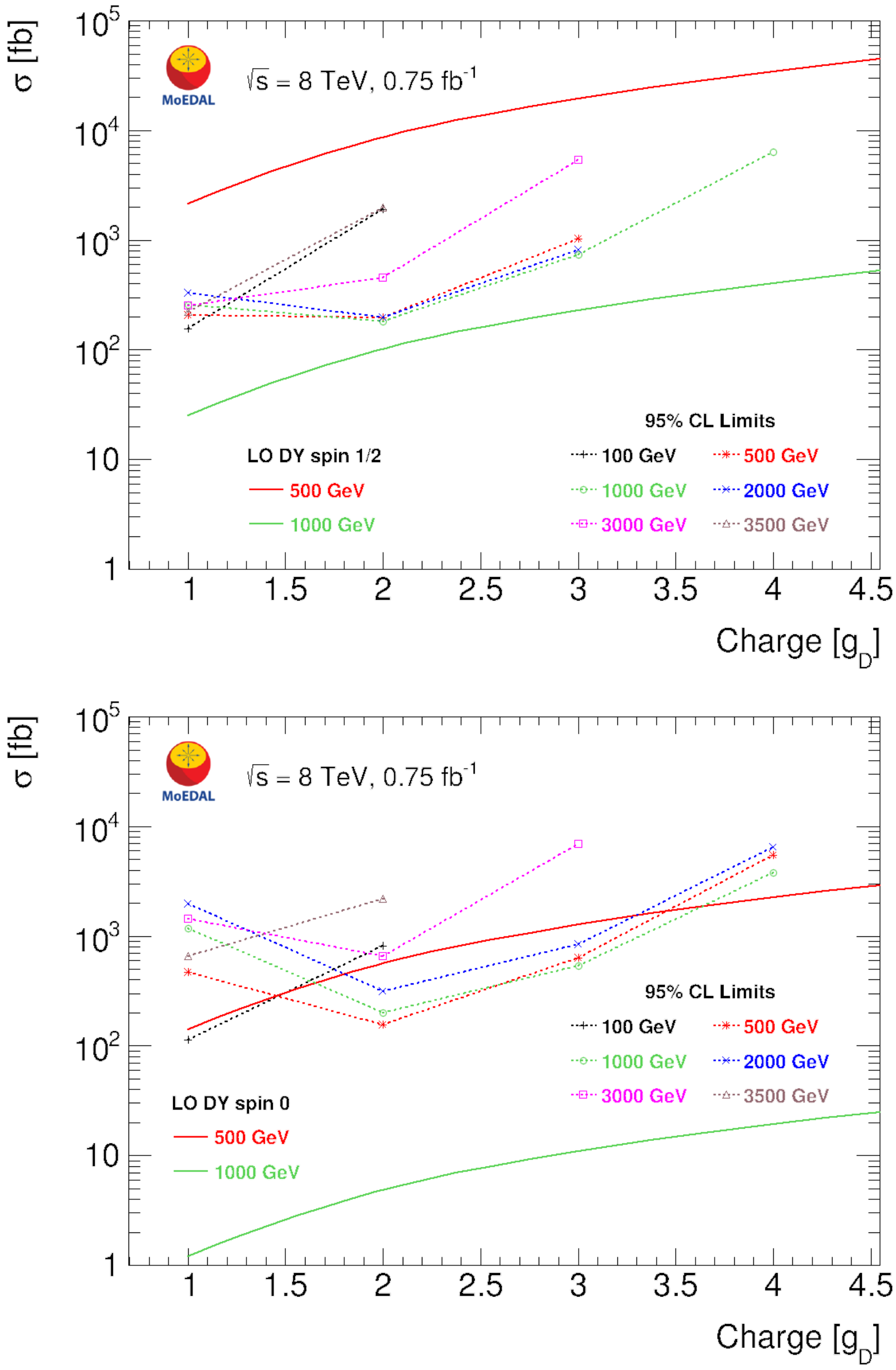

Figure 9. Cross-section upper limits at 95% confidence level for leading-order DY monopole production as a function of charge for spin-1/2 (top) and spin-0 (bottom) monopoles. The various line styles correspond to different monopole masses. The solid lines are DY cross section calculations at leading order.

DY Lower Mass Limits [GeV]	$\lvert g \rvert = g_D$	$\lvert g \rvert = 2g_D$	$\lvert g \rvert = 3g_D$
spin-1/2	710	940	805
spin-0	510	610	550

Table 2. Lower mass limits in models of spin-1/2 (top) and spin-0 (bottom) DY monopole pair production. These limits are based upon cross sections computed at leading order. They are only indicative since the monopole coupling to the photon is too large to allow for perturbative calculations.

Table. 2 for magnetic charges up to $3g_D$ for spin-1/2 and spin-0 DY monopoles. The mass limits obtained for $|g| = g_D$ are comparable to although not quite as stringent as the recent ATLAS results at 8 TeV [22]. The mass limits for $|g| = 2g_D$ and $|g| = 3g_D$ are the first to date at the LHC and surpass the results from previous collider experiments.

6 Conclusions

MoEDAL is designed for passive detection of magnetic monopoles, both in-flight (with the track-etch technique) and trapped (with the induction technique, as in this work). A pioneering search for trapped magnetic monopoles was performed using a trapping detector prototype exposed to 0.75 fb^{-1} of 8 TeV proton-proton collisions in 2012. This is the first time in history that a dedicated scalable and recyclable monopole trapping array has been deployed at an accelerator facility. Full scanning of this array with a superconducting magnetometer was performed and no monopoles with magnetic charge $\geq 0.5g_D$ were found in any of the samples. Under the assumption of monopole capture by aluminium nuclei, this results in 95% confidence level cross section limits ranging from 100 fb to 6000 fb in models of DY monopole pair production for charges up to $4g_D$ and masses up to 3500 GeV (while previous LHC contraints for pair production exist only for $|g| \leq 1.5g_D$ and $m \leq 2500$ GeV). Under the additional assumption of a DY cross section at leading order, mass limits are obtained for magnetic charges up to $3g_D$. A limit of 10 fb is also set for monopoles with charges up to $6g_D$ and masses up to 3500 GeV produced in fiducial regions of longitudinal kinetic energy and polar angle for which they have a relatively constant 40% probability to be trapped.

Despite a small solid angle coverage and modest luminosity, the MoEDAL trapping detector probes ranges of charge, mass and energy which could not be accessed by other LHC experiments. Furthermore, this technique can yield results very quickly and would allow for an unambiguous background-free assessment of a signal, potentially providing a direct measurement of a monopole magnetic charge based on its electromagnetic properties only. A new, larger trapping detector array was deployed in 2014 along the back and rear of the LHCb VELO vessel, allowing to perform a search in 13 TeV collisions in the near future.

Acknowledgements

This work was supported by a fellowship from the Swiss National Science Foundation and a grant from the Marc Birkigt Fund of the Geneva Academic Society.

References

[1] P. Dirac, *Quantised Singularities in the Electromagnetic Field*, *Proc. Roy. Soc.* **A 133** (1931) 60.

[2] G. 't Hooft, *Magnetic Monopoles in Unified Gauge Theories*, *Nucl. Phys. B* **79** (1974) 276.

[3] A. Polyakov, *Particle Spectrum in the Quantum Field Theory*, *JETP Lett.* **20** (1974) 194.

[4] Y. Cho and D. Maison, *Monopole configuration in Weinberg-Salam model*, *Phys. Lett. B* **391** (1997) 360, [9601028].

[5] T. Kirkman and C. Zachos, *Asymptotic Analysis of the Monopole Structure*, *Phys. Rev. D* **24** (1981) 999.

[6] J. Schwinger, *Magnetic charge and the charge quantization condition*, *Phys. Rev. D* **12** (1975) 3105.

[7] S. Ahlen, *Stopping-power formula for magnetic monopoles*, *Phys. Rev. D* **17** (1978) 229.

[8] S. Ahlen, *Theoretical and experimental aspects of the energy loss of relativistic heavily ionizing particles*, *Rev. Mod. Phys.* **52** (1980) 121.

[9] S. Ahlen and K. Kinoshita, *Calculation of the stopping power of very-low-velocity magnetic monopoles*, *Phys. Rev. D* **26** (1982) 2347.

[10] K. Milton, *Theoretical and experimental status of magnetic monopoles*, *Rep. Prog. Phys.* **69** (2006) 1637, [0602040].

[11] OPAL Collaboration, *Search for Dirac magnetic monopoles in* e^+e^- *collisions with the OPAL detector at LEP2*, *Phys. Lett. B* **663** (2008) 37, [arXiv:0707.0404].

[12] CDF Collaboration, *Direct search for Dirac magnetic monopoles in* $p\bar{p}$ *collisions at* $\sqrt{s} = 1.96$ *TeV*, *Phys. Rev. Lett.* **96** (2006) 201801, [0509015].

[13] J. Pinfold, *Searching for the magnetic monopole and other highly ionizing particles at accelerators using nuclear track detectors*, *Radiat. Meas.* **44** (2009) 834.

[14] K. Kinoshita, R. Du, G. Giacomelli, L. Patrizii, F. Predieri, P. Serra, M. Spurio, and J. Pinfold, *Search for highly ionizing particles in* e^+e^- *annihilations at sqrt(s) = 91.1 GeV*, *Phys. Rev. D* **46** (1992) 881.

[15] J. Pinfold, R. Du, K. Kinoshita, B. Lorazo, M. Regimbald, and B. Price, *A Search for highly ionizing particles produced at the OPAL intersection point at LEP*, *Phys. Lett. B* **316** (1993) 407.

[16] M. Bertani, G. Giacomelli, M. Mondardini, B. Pal, L. Patrizii, F. Predieri, P. Serra-Lugaresi, G. Sini, M. Spurio, V. Togo, and S. Zucchelli, *Search for Magnetic Monopoles at the Tevatron Collider*, *Europhys. Lett.* **12** (1990) 613.

[17] H1 Collaboration, *A direct search for stable magnetic monopoles produced in positron-proton collisions at HERA*, *Eur. Phys. J. C* **41** (2005) 133, [0501039].

[18] G. Kalbfleisch, K. Milton, M. Strauss, L. Gamberg, E. Smith, and W. Luo, *Improved Experimental Limits on the Production of Magnetic Monopoles*, *Phys. Rev. Lett.* **85** (2000) 5292, [0005005].

[19] G. Kalbfleisch, W. Luo, K. Milton, E. Smith, and M. Strauss, *Limits on production of magnetic monopoles utilizing samples from the D0 and CDF detectors at the Tevatron*, *Phys. Rev. D* **69** (2004) 052002, [0306045].

[20] A. De Roeck, A. Katre, P. Mermod, D. Milstead, and T. Sloan, *Sensitivity of LHC experiments to exotic highly ionising particles*, *Eur. Phys. J. C* **72** (2012) 1985, [arXiv:1112.2999].

[21] ATLAS Collaboration, *Search for magnetic monopoles in sqrt(s) = 7 TeV pp collisions with the ATLAS detector*, *Phys. Rev. Lett.* **109** (2012) 261803, [arXiv:1207.6411].

[22] ATLAS Collaboration, *Search for magnetic monopoles and stable particles with high electric charges in 8 TeV pp collisions with the ATLAS detector*, *submitted to Phys. Rev. D* (2015) [arXiv:1509.08059].

[23] A. De Roeck, H.-P. Hächler, A. M. Hirt, M. Dam Joergensen, A. Katre, P. Mermod, D. Milstead, and T. Sloan, *Development of a magnetometer-based search strategy for stopped monopoles at the Large Hadron Collider*, *Eur. Phys. J. C* **72** (2012) 2212, [arXiv:1206.6793].

[24] MoEDAL Collaboration, *The Physics Programme Of The MoEDAL Experiment At The LHC*, *Int. J. Mod. Phys. A* **29** (2014) 1430050, [arXiv:1405.7662].

[25] LHCb Collaboration, *The LHCb Detector at the LHC*, *JINST* **3** (2008) S08005.

[26] K. Bendtz, D. Milstead, H.-P. Hachler, A. Hirt, P. Mermod, P. Michael, T. Sloan, C. Tegner, and S. Thorarinsson, *Search for magnetic monopoles in polar volcanic rocks*, *Phys. Rev. Lett.* **110** (2013) 121803, [arXiv:1301.6530].

[27] J. Clarke and A. Braginski, *The SQUID Handbook: Fundamentals and Technology of SQUIDs and SQUID Systems*, *Wiley* (2006).

[28] J. Alwall, M. Herquet, F. Maltoni, O. Mattelaer, and T. Stelzer, *MadGraph 5 : Going Beyond*, *JHEP* **06** (2011) 128, [arXiv:1106.0522].

[29] R. D. Ball et al., *Parton distributions with LHC data*, *Nucl. Phys. B* **867** (2013) 244, [arXiv:1207.1303].

[30] T. Sjostrand, S. Mrenna, and P. Z. Skands, *A Brief Introduction to PYTHIA 8.1*, *Comput. Phys. Commun.* **178** (2008) 852, [arXiv:0710.3820].

[31] Geant4 Collaboration, *Geant4 developments and applications*, *IEEE Trans. Nucl. Sci.* **53** (2006) 270.

[32] ATLAS Collaboration, *Search for massive long-lived highly ionising particles with the ATLAS detector at the LHC*, *Phys. Lett. B* **698** (2011) 353, [arXiv:1102.0459].

[33] I. Bertram, G. L. Landsberg, J. Linnemann, R. Partridge, M. Paterno, and H. B. Prosper, *A Recipe for the construction of confidence limits*, *FERMILAB-TM-2104* (2000).